

Use of surface plasmons for manipulation of organic molecule quasiparticles and optical properties

This content has been downloaded from IOPscience. Please scroll down to see the full text.

2014 J. Phys.: Condens. Matter 26 485012

(<http://iopscience.iop.org/0953-8984/26/48/485012>)

View [the table of contents for this issue](#), or go to the [journal homepage](#) for more

Download details:

IP Address: 158.227.181.29

This content was downloaded on 13/11/2014 at 12:39

Please note that [terms and conditions apply](#).

Use of surface plasmons for manipulation of organic molecule quasiparticles and optical properties

V Despoja^{1,2} and L Marušić³

¹ Department of Physics, University of Zagreb, Bijenička 32, HR-10000 Zagreb, Croatia

² Donostia International Physics Center (DIPC), Paseo de Manuel de Lardizabal 4, ES-20018 San Sebastián, Spain

³ Maritime Department, University of Zadar, M. Pavlinovića b.b., HR-23000 Zadar, Croatia

E-mail: vito@phy.hr and lmarusic@unizd.hr

Received 28 July 2014, revised 20 October 2014

Accepted for publication 24 October 2014

Published 12 November 2014

Abstract

Our recently proposed theoretical formulation based on Bethe–Salpeter G_0W_0 methodology is applied here to explore the quasiparticle and optical spectra of anthracene ($C_{14}H_{10}$) placed close to a metallic surface. Special attention is paid to explore how the energy shift and decay width of the low-lying anthracene bright excitons p , α and β depend on the type of the adjacent surface (described by the Wigner Seitz radius r_s) and the separation from the surface. It is shown that p and α excitons weakly interact with surface excitations, but for $r_s \approx 3$ the intensive β exciton hybridizes with surface plasmon considerably, resulting in its splitting into two optically active modes. The β exciton decays extraordinarily fast ($\Gamma \approx 200$ meV) to the electron–hole excitations in the metallic surface even for non-contact separations ($z_0 \approx 12$ a.u.). For $r_s > 5$ the β exciton becomes infinitely sharp ($\Gamma \approx 0$) and no longer interacts with the surface plasmon. Moreover, it is shown that HOMO and LUMO states near a metallic surface behave as statically screened rigid orbitals, with the result that the simple image theory arguments are sufficient to explain the HOMO–LUMO gap shift. Finally, it is demonstrated that the HOMO–LUMO gap shift dominantly depends on the position of the effective image plane z_{im} of the adjacent surface.

Keywords: surface plasmons, optical spectra, organic molecule

(Some figures may appear in colour only in the online journal)

1. Introduction

Organic molecular crystals (layers) or polymers deposited on metallic nanoparticles are increasingly being experimentally tested in order to explore their suitability for applications in organic photovoltaics, organic electronic circuits, organic transistors, biosensing, etc [1–5]. Organic π conjugated molecules have been proven to be the best candidates for all these applications. The molecule that has recently been studied extensively is anthracene ($C_{14}H_{10}$) and its derivatives. For example, some anthracene derivatives have recently been successfully tested as donor materials in organic photovoltaic [6–10]. Even though a lot of work has been performed dealing with individual molecules, there is a lack of theoretical studies

that explore the molecular electronic structure, excitation spectra or optical absorption spectra when a molecule is deposited on a substrate. This is because the numerical complications become enormous. In this paper we focus on quasiparticles and the optical properties of anthracene placed close to a metallic surface. Molecular ground and excitation properties are obtained combining *ab initio* molecular orbitals and solving a G_0W_0 -Bethe Salpeter (G_0W_0 BSE) scheme. For the metallic surface we use a *jellium* model. The main objective is to explore how the low-lying anthracene excitons interact with electronic modes in the metallic surface. Due to the weak intermolecular binding in the anthracene crystal (with absorption spectra very similar to gas phase absorption

spectra), the results and the conclusions obtained for the isolated molecule can also be considered relevant for an anthracene monolayer in the vicinity of a metallic surface.

In this theoretical investigation we shall use the formulation developed in our recent paper [11] which is mostly based on previous well established and tested theories that combine the Bethe–Salpeter equation (BSE) and the G_0W_0 method for the determination of the quasiparticle properties of a molecule [12–18]. However, the theoretical method presented in [11] has been modified. Specifically, the molecular optical spectra are obtained directly from the imaginary part of the dynamical 4-point polarizability matrix $L_{ij}^{kl}(\omega)$, which is the solution of the matrix BSE. The formulation is also extended in order to include the interaction of the molecule with the metallic surface. For an isolated molecule, the interaction between charge fluctuations is mediated by a bare Coulomb potential V , but for a molecule in the vicinity of a metallic surface, the interaction becomes mediated by screened Coulomb potential $\tilde{W}(\omega) = V + \Delta W(\omega)$, where $\Delta W(\omega)$ is the RPA induced Coulomb interaction which describes the substrate polarizability while molecular excitation is described within BSE- G_0W_0 . In this way, we can obtain an accurate description of the molecule/surface interactions at reasonable computational cost [11, 19] and perform computational screening of the optical absorption and inter-facial coupling of a molecule near a surface.

First we calculate the quasiparticle spectra and optical spectra of isolated (gas phase) anthracene, compare them with available theoretical and experimental results and find that the calculated HOMO–LUMO gap is in excellent agreement with the experimental result [20]. The calculated optical absorption spectra show three lowlying excitons $^1B_{3u}(x, p)$, $^1B_{2u}(y, \alpha)$ and the most intensive $^1B_{2u}(y, \beta)$, throughout the paper denoted as p , α and β excitons, respectively. The energies of the p , α and β excitons slightly overestimate the experimental values [21, 22].

The second step is a detailed analysis of the influence of different *jellium* surfaces (different Wigner Seitz radius r_s) on the molecular quasiparticle and optical spectra and for different distances between the molecule and the surfaces. Even though the adsorption of anthracene on noble metal surfaces has already been experimentally studied [23, 24] there is still a lack of experimental studies dealing with the influence of a metallic substrate on molecular quasiparticles and absorption spectra. We show here that for particular surfaces ($r_s \approx 3$) the β exciton strongly hybridizes with surface plasmons in such a way that the β exciton splits into two equally intensive peaks which are both optically active. The surface reduces the HOMO–LUMO gap such that HOMO and LUMO states behave as rigid statically screened orbitals, and the dynamical effects are irrelevant. We demonstrate how different metallic surfaces, i.e. different r_s , influence the HOMO–LUMO gap. We show how the HOMO–LUMO gap changes the effective image plane z_{im} as a function of r_s . Finally, we show that the β exciton strongly decays to electron–hole excitations in the metallic surface, and the β exciton decay width Γ decreases with molecule surface separation z_0 . The p and α excitons are weakly affected by the metallic substrate.

Most of the aromatic hydrocarbons, when deposited on metallic substrates, prefer planar geometry, and the equilibrium separations are about 6–7 a.u. from the topmost metal atomic layer. This motivated us to choose the anthracene plane to lie parallel to the metallic surface and at a minimum distance 6 a.u. from the surface. However, some molecules, such as pentacene on Au(1 1 1) [25], favour the sideways configuration. Also, even if the molecule prefers the parallel configuration, the substrate could cause the molecular bending or the inclination of the CH bond (with respect to the molecular plane), e.g. in benzene on Pt(1 1 1) [26]. All this structural deformation can substantially influence the quasiparticle and optical spectra of the deposited molecule, or the exciton–surface plasmon hybridization. However, in most cases, e.g. pentacene on Ag(1 1 1) [27], benzene on graphene [11] or benzene on Au(1 1 1) [26], the substrate’s influence on the parallel molecular structure and energy levels is weak (within the DFT approach). Also, the lateral position of the molecule is unimportant. This allows us to treat the molecules and the substrates as independent objects (on DFT level) and to describe the substrate by some relatively simple model (e.g. a *jellium* model), as is done in [11, 28]. However, this paper does not aim to investigate how ‘realistically’ the substrate modifies molecular structure and orientation, and consequently its optical spectrum. We restrict our investigation to a more simple model where we freeze the molecular structure and investigate how the substrate screening influences the molecular optical and quasiparticle spectra as a function of the molecule—substrate separation and the substrate density.

In section 2 we briefly present the methodology used to obtain the 4-point polarizability matrix $L_{ij}^{kl}(\omega)$, and then show how $L_{ij}^{kl}(\omega)$ can be applied to calculate optical absorption spectra of isolated molecules and of the molecule in the vicinity of a metallic surface. In section 3 we present the results for the HOMO–LUMO gap and optical absorption spectra of anthracene in the vicinity of a metallic surface, for various surfaces (various r_s) and various separations between the molecule and the surface. This is followed by concluding remarks in section 4.

2. Formulation of the problem

An incident light beam can create an electron–hole pair in a molecule and, in the lowest approximation, the motion of the pair can be considered as two independent particles propagating through the molecule without any mutual interactions. Such a long lived electron–hole pair propagation can be described as a convolution of two one-particle Green’s functions which can be calculated within a local density approximation (LDA) Kohn–Sham (KS) scheme [29]. However, the excited electron and hole can still interact with other molecular excitations, e.g. collective electronic modes (plasmons) or molecular vibrational modes (phonons). Such additional interactions, especially long range electron–electron correlations, are not included at the LDA level and one particle Green’s function must be corrected in order to include all these effects. Moreover, because of the electron–electron interaction, excited electrons and holes can interact

mutually or annihilate and interact with other electron–hole excitations in the molecule. Therefore, in order to obtain accurate molecular excitation spectra, all of these processes should be carefully taken into account. To do this we calculate full electron–hole propagator or 4-point polarizability L , following the BSE approach, described in detail in our previous publications [11, 30].

We obtain the 4-point polarizability matrix L_{ij}^{kl} as the solution of the Bethe–Salpeter equation [11]

$$L_{ij}^{kl}(\omega) = \tilde{L}_{ij}^{kl}(\omega) + \sum_{i_1 j_1 k_1 l_1} \Theta_{i_1 j_1}^{k_1 l_1} \tilde{L}_{ij}^{i_1 j_1}(\omega) \Xi_{i_1 j_1}^{k_1 l_1} L_{k_1 l_1}^{kl}(\omega), \quad (1)$$

where the prefactor

$$\Theta_{ij}^{kl} \equiv |f_j - f_i| |f_l - f_k|, \quad (2)$$

ensures that only the transitions between empty and filled molecular states contribute. \tilde{L}_{ij}^{kl} is the noninteracting quasiparticle 4-point polarizability matrix calculated using the quasiparticle energies $\tilde{\epsilon}_i$ obtained by solving the Dyson equation, where the exchange–correlation self-energy operator is calculated within $G_0 W_0$ approximation [11, 30]:

$$\Sigma_{XC}(\mathbf{r}, \mathbf{r}', \omega) = i \int_{-\infty}^{\infty} \frac{d\omega'}{2\pi} e^{-i\omega'\delta} G_0(\mathbf{r}, \mathbf{r}', \omega - \omega') \times W_0(\mathbf{r}, \mathbf{r}', \omega'). \quad (3)$$

This approach is referred to as the BSE- $G_0 W_0$ scheme, and the BSE kernel [30]

$$\Xi_{ij}^{kl} = \Xi_{ij}^{kl,H} - \Xi_{ij}^{kl,F} \quad (4)$$

consists of Hartree and Fock terms

$$\Xi_{ij}^{kl,H} = \int d\mathbf{r}_1 d\mathbf{r}_2 \phi_i^j(\mathbf{r}_1) V(\mathbf{r}_1 - \mathbf{r}_2) \phi_l^k(\mathbf{r}_2) \quad (5)$$

and

$$\Xi_{ij}^{kl,F} = \frac{1}{2} \int d\mathbf{r}_1 d\mathbf{r}_2 \phi_i^j(\mathbf{r}_1) W(\mathbf{r}_1, \mathbf{r}_2, \omega = 0) \phi_l^k(\mathbf{r}_2), \quad (6)$$

where $V(\mathbf{r}_1 - \mathbf{r}_2)$ is the propagator of the bare Coulomb interaction and

$$\phi_i^j(\mathbf{r}) = \psi_i^*(\mathbf{r}) \psi_j(\mathbf{r}), \quad (7)$$

Our aim is to simulate an optical absorption experiment, i.e. the situation when an incident electromagnetic wave couples to the electronic excitations in the system and is partially absorbed. We shall calculate the absorption spectra $P(\omega)$ within the linear response theory which again is described in our previous publications [11, 30], and links the spectra to the 4-point polarizability matrix

$$P(\omega) = -\omega \text{Im} \left\{ \sum_{ijkl} \Theta_{ij}^{kl} L_{ij}^{kl}(\omega) J_{ji} J_{kl} \right\}, \quad (8)$$

where $J_{ji} J_{kl}$ are current vertices [31].

The system we want to investigate is anthracene placed close to a metallic surface, as illustrated in figure 1. The incident electromagnetic field induces molecular currents,

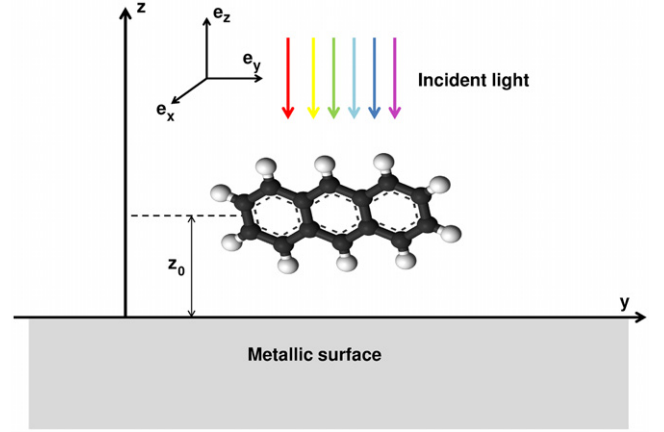


Figure 1. Schematic illustration of the optical absorption experiment on anthracene close to the metallic surface.

and if the molecule is placed close to a conducting surface these currents can induce charge density fluctuation in the surface. Induced surface charge then produces a field which screens interaction between charge density fluctuations in the molecule causing renormalization of the molecular optical and quasiparticle spectra. In order to take into account the modifications caused by the polarization of the metallic surface, we need to modify the BSE- $G_0 W_0$ scheme. The metallic plane is chosen to be parallel to the xy -plane, i.e. to be perpendicular to the z -axis. The ground state electronic structure of the surface is treated in the *jellium* model [29] where we chose a *jellium* edge to be located at $z = 0$. For the molecular plane (benzene rings plane), we chose for it to lie parallel to the metallic plane. The distance between the anthracene plane and the *jellium* edge is denoted by z_0 , as shown in figure 1. Many recent vdW-DF studies of aromatic hydrocarbons deposited parallel to metallic substrates show that the equilibrium molecule–substrate separation is between 6.0–7.0 a.u. [11, 25–27] For this separation the electronic density overlap is negligible, as can be seen e.g. in figure 11 of [11]. This calculation is performed for $z_0 > 6$ a.u. to ensure that the molecular and surface electronic densities do not overlap, which simplifies the impact of the metal surface significantly, reducing it to the calculation of the 4-point polarizability matrix. More specifically, since there is no inter-system electron hopping, the molecule and surface can be treated as two separate systems which can polarize each other through the long range Coulomb interaction. From a molecular point of view, this means that all the interactions propagating inside the molecule have to be additionally screened because of the polarization of the surface. To achieve this, the bare Coulomb interaction inside the molecule, used for the calculation of Hartree (5) and Fock (6) BSE kernels, as well as for the calculation of the exchange–correlation self energy (3) for the single particle propagator, should be renormalized as

$$V(\mathbf{r}, \mathbf{r}') \rightarrow \tilde{W}(\mathbf{r}, \mathbf{r}', \omega) = V(\mathbf{r}, \mathbf{r}', \omega) + \Delta W(\mathbf{r}, \mathbf{r}', \omega), \quad (9)$$

where ΔW represents the substrate contribution to the induced Coulomb interaction [11] which can be Fourier transformed in

the xy -plane

$$\Delta W(\mathbf{r}, \mathbf{r}', \omega) = \int \frac{d\mathbf{Q}}{(2\pi)^2} e^{i\mathbf{Q}(\rho-\rho')} \Delta W(\mathbf{Q}\omega, z, z'), \quad (10)$$

where $\rho = (x, y)$ and $\mathbf{Q} = (Q_x, Q_y)$ is a two-dimensional wave vector. In the region $z, z' > 0$ anthracene feels an ‘external’ metallic field with the spatial part of the Fourier transform (10) of simple form [29, 32]

$$\Delta W(\mathbf{Q}, \omega, z, z') = D(Q, \omega) e^{-Q(z+z')}, \quad (11)$$

where the surface excitation propagator $D(Q, \omega)$ contains the intensities of all (collective and single particle) electronic excitations in the metallic surface. Calculation of the propagator $D(Q, \omega)$ is described in detail in [29, 32], and here we shall only describe it briefly. First we suppose that metal is translationally invariant in the direction parallel to the surface, i.e. that the electron wave function in that direction are plane waves with energies $\frac{\hbar^2 \mathbf{K}^2}{2m}$, and $\mathbf{K} = \{K_x, K_y\}$ is a 2D wave vector. In z direction where the symmetry is broken the system is described by Kohn–Sham wave functions $\phi_n(z)$ and energy levels E_n which are self-consistent solutions of the one-dimensional Kohn–Sham equation for the 150 a.u. thick *jellium* slab. The positive background density is defined by the Wigner Seitz radius r_s [33]. For the exchange and correlation potential we use the LDA Wigner formula. First we calculate the Fourier transform of the non-interacting electron response function $\chi_0(Q, \omega, z, z')$, constructed from Kohn–Sham wave functions $\phi_n(z)$ and energy levels E_n . Therefore, intraband $n = m$ contributions to χ_0 are similar to quasi 2D Lindhard functions, but we also include the interband $n \neq m$ contributions. The screened response function $\chi(Q, \omega, z, z')$ is calculated from χ_0 by solving the matrix equation $\chi = \chi_0 + \chi_0 V \chi$ where, at an RPA level of approximation, V is the 2D Fourier transform of the bare Coulomb interaction $V(Q) = \frac{2\pi}{Q} e^{-Q|z-z'|}$. Propagator $D(Q, \omega)$ represents an induced dynamically screened Coulomb interaction at the metallic surface, which can be simply obtained from the screened response function $\chi(Q, \omega, z, z')$ as

$$\begin{aligned} D(Q, \omega) &= \frac{1}{v_Q} W^{\text{ind}}(Q, \omega, z=0, z'=0) \\ &= v_Q \int dz_1 dz_2 e^{Q(z_1+z_2)} \chi(Q, \omega, z_1, z_2). \end{aligned}$$

Interactions with the surface also renormalize the quasiparticle energy levels $\tilde{\epsilon}_i$. In the lowest order approximation, this can be done by correcting the self energy operator (3) by the induced self energy operator

$$\begin{aligned} \Delta \Sigma_{XC}(\mathbf{r}, \mathbf{r}', \omega) &= \\ i \int_{-\infty}^{\infty} \frac{d\omega'}{2\pi} e^{-i\omega'\delta} \tilde{G}_0(\mathbf{r}, \mathbf{r}', \omega - \omega') \Delta W(\mathbf{r}, \mathbf{r}', \omega'). \end{aligned} \quad (12)$$

This implies that the induced self energy of the i th state becomes

$$\Delta \Sigma_i^{\text{XC}}(\omega) = \Delta \Sigma_i^{\text{X}}(\omega) + \Delta \Sigma_i^{\text{C}}(\omega), \quad (13)$$

where the induced exchange self energy becomes

$$\Delta \Sigma_i^{\text{X}}(\omega) = - \sum_{j=1}^N \Delta W_{ij}^{ij}(\omega - \tilde{\epsilon}_j) \quad (14)$$

and the induced correlation term is

$$\Delta \Sigma_i^{\text{C}}(\omega) = - \frac{1}{\pi} \sum_{j=1}^{\infty} \int_0^{\infty} d\omega' \frac{\text{Im} \{ \Delta W_{ij}^{ij}(\omega') \}}{\omega - \tilde{\epsilon}_j - \omega' + i\eta}. \quad (15)$$

The induced Coulomb interaction matrix elements that should be added to Hartree and Fock kernels (5) and (6) are then

$$\Delta W_{ij}^{kl}(\omega) = \int_{\Omega_{\text{cell}}} d\mathbf{r}_1 d\mathbf{r}_2 \phi_i^j(\mathbf{r}_1) \Delta W(\mathbf{r}_1, \mathbf{r}_2, \omega) \phi_l^k(\mathbf{r}_2). \quad (16)$$

Note that the Green’s function appearing in (12) is the renormalized Green’s function \tilde{G}_0 calculated with the use of the quasiparticle eigen-energies $\tilde{\epsilon}_i$ obtained for the isolated molecule. Accordingly, the renormalized quasiparticle energy levels $\tilde{\epsilon}_j$ also appear in (14) and (15).

3. Results and discussion

The anthracene Kohn–Sham orbitals $\psi_i(\mathbf{r})$ and energy levels ϵ_i are obtained by using the plane-wave self-consistent field density functional theory (DFT) code (PWscf), within the Quantum Espresso (QE) package [34], using the Perdew–Wang GGA (PW91) exchange and correlation (XC)-functional [35]. We model the molecule using a periodically repeated $45.69 a_0 \times 45.69 a_0 \times 45.69 a_0$ unit cell. Since there is no intermolecular overlap, the ground state electronic density is calculated at the Γ point only. For hydrogen and carbon atoms we used GGA-based ultra soft pseudo potentials⁴, and found the energy spectrum to be convergent with a 30 Ry plane-wave cutoff. The two-dimensional \mathbf{Q} integration in (10) is performed using a 61×61 rectangular mesh and the cutoff wave vector $Q_C = 0.3$ a.u.

To calculate the quasiparticle eigenvalues $\tilde{\epsilon}_i$ within G_0W_0 approximation for the isolated anthracene molecule, one must include an increased number of unoccupied states in both, the summation over unoccupied states in Σ_C and calculation of the screened interaction W . The anthracene molecule has 66 valence electrons, i.e. 33 doubly occupied valence orbitals. We found that including 144 bands, i.e. 4.6 unoccupied bands per atom, is sufficient to obtain converged values for $\tilde{\epsilon}_i$. The RPA screened Coulomb interaction W used to calculate G_0W_0 contains high energy plasmon-like $\pi \rightarrow \sigma^*$ and $\sigma \rightarrow \sigma^*$ excitations located in the energy region between 15–20 eV. This means that the integration in Σ_C includes the majority of the anthracene spectral weight which provides converged values for quasiparticle eigenvalues $\tilde{\epsilon}_i$.

Since p , α and β excitons mostly consist of $\pi \rightarrow \pi^*$ transition in the HOMO–LUMO region [20–22] we used a significantly reduced base set of 5 occupied and 5 unoccupied states, i.e. the base set

⁴ All pseudopotentials are available free of charge via the Internet at www.quantum-espresso.org/pseudopotentials.

{HOMO – 4, HOMO – 3, ..., LUMO + 4} to determine the 4-point polarizability, i.e. to solve solving BSE (1).

Since we study a single isolated anthracene molecule, we have to exclude the effect on its polarizability due to the interaction with surrounding molecules in the lattice. This is accomplished by solving the BSE with use of the truncated Coulomb interaction [36]

$$V_C(\mathbf{r} - \mathbf{r}') = \frac{\Theta(|\mathbf{r} - \mathbf{r}'| - R_C)}{|\mathbf{r} - \mathbf{r}'|}, \quad (17)$$

where Θ is the Heaviside step function, and R_C is the range of the Coulomb interactions, i.e. the radial cutoff. Since we choose the lattice constant $L = 45.69 a_0$ to be more than twice the range of the anthracene molecule's density, choosing the radial cutoff to be $R_C = L/2$ ensures that the charge fluctuations created within the molecule produce a field throughout the whole molecule but do not produce any field that could influence the surrounding molecules. The definition (17) is very useful because the Coulomb interaction remains translationally invariant.

First, we calculate the quasiparticle spectra and optical spectra of isolated (gas phase) anthracene and compare them with the available theoretical and experimental results. The calculated quasiparticle HOMO–LUMO gap 6.82 eV is in very good agreement with the experimental result 6.91 eV [20]. We calculated the optical absorption spectrum of the isolated molecule in order to explore the energies of the low-lying excitons. It is well known that isolated anthracene supports three low-lying optically active modes: $^1B_{3u}(x, p)$ or p mode—polarized along shorter molecular axis, $^1B_{2u}(y, \alpha)$ or α mode—polarized along a longer molecular axis, and the most intensive $^1B_{2u}(y, \beta)$ or β mode—also polarized along a longer molecular axis [21]. The experimental energies of the p , α and β modes are 3.43 eV, 3.84 eV and 5.24 eV, respectively [21], though [22] reports slightly lower values for each of the excitons. Our calculations, obtained by using (8), give peaks at 3.7 eV, 4.2 eV and 5.9 eV which overestimates the experimental values by 8%, 9% and 12%, for the p , α and β mode, respectively. A possible reason for this overestimation could be that in the final stage of calculation, where we solve the BSE equation, we take into account only the excitations within the $\pi \rightarrow \pi^*$ sector which distorts the f-sum rule. However, our recent studies performed for benzene and fullerene [11, 30] (which also include only the transitions within $\pi \rightarrow \pi^*$ sector) have given satisfactory results for all kinds of low energy excitons. Moreover, we performed separated calculations here in which the BSE is additionally screened by transitions within the $\pi \rightarrow \sigma^*$ and $\sigma \rightarrow \sigma^*$ sector, but that did not change the position of the low-lying excitons. Therefore the effect responsible for the overestimation of exciton energy is probably beyond the approximations used in this investigation.

Figure 2 shows anthracene optical absorption intensities as functions of incident electromagnetic field frequency ω and Wigner Seitz radius r_s of the electron gas in the adjacent *jellium* surface. The graph on the bottom corresponds to $r_s = 2$ and for each subsequent graph r_s increases by 0.2, so the graph on the top shows a spectrum for $r_s = 5$. The separation between the molecule plane and the *jellium* edge ($z = 0$) is

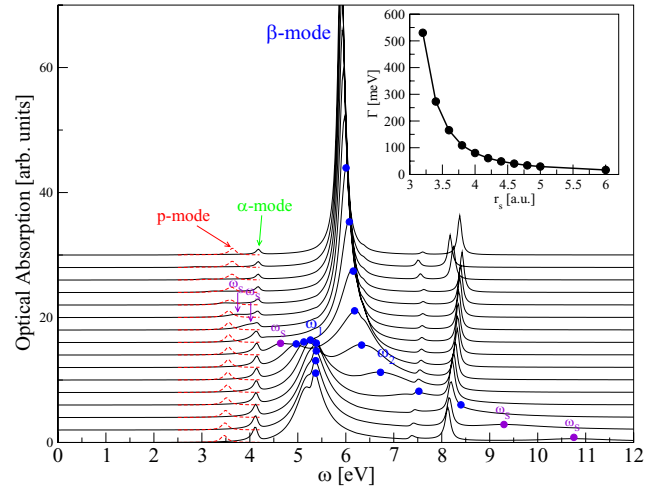


Figure 2. Anthracene optical absorption spectra as functions of the incident light frequency ω for various Wigner Seitz radii $r_s = 2, 2.2, 2.4, \dots, 5$ (from bottom to top) of the electron gas in the adjacent *jellium* surface. Black solid lines: incident light polarized along the long molecular axis (y). Red dashed lines: incident light polarized along the short molecular axis (x) (red/dashed lines). The separation between the molecular plane and the *jellium* edge is chosen to be $z_0 = 6$ a.u. Inset: β exciton decay width Γ as a function of the Wigner Seitz radius r_s .

chosen to be $z_0 = 6$ a.u. Black (solid) lines represent the absorption intensities, obtained using (8), when the incident electromagnetic field is y -polarized. Peaks appearing in these spectra correspond to α and β excitons. Red (dashed) lines represent the low energy part of the absorption spectra, obtained using (8), when the incident electromagnetic field is x -polarized, i.e. it shows the positions of the p exciton or the molecular optical gap.

The graphs clearly show that the presence of a surface substantially influences the β exciton, while the p and α excitons remain almost unaffected. The influence of the surface increases as with the increasing electron density, i.e. decreasing Wigner Seitz radius r_s , so the graphs should be observed from top to bottom. In the top graphs we can clearly see a very strong β exciton and weaker but noticeable p and α excitons. As the r_s decreases, the surface plasmon (denoted as ω_s and marked with purple arrows/dots) appears and moves towards higher frequencies. For higher values of r_s , the surface plasmon peak is very weak and it passes the p and α exciton modes without affecting them. However, for r_s below 3.4 the surface plasmon becomes more prominent and approaches the β exciton, so in the region $2.8 < r_s < 3.2$ the plasmon peak becomes comparable to the β exciton, and strong hybridization between these modes can be observed. At first (r_s around 3.4) this can be seen as pushing the β exciton towards higher energies and the surface plasmon towards lower energies (as the r_s decreases) and then, for lower r_s , we can see two hybridized modes (denoted as ω_1 and ω_2) with different parity, which cannot be clearly distinguished as either a surface plasmon or a β exciton. Detailed examination of the electron density distribution (not presented in this paper) shows that, unlike the excitons (located within the molecule) and the plasmons (located within the surface), these excitations are

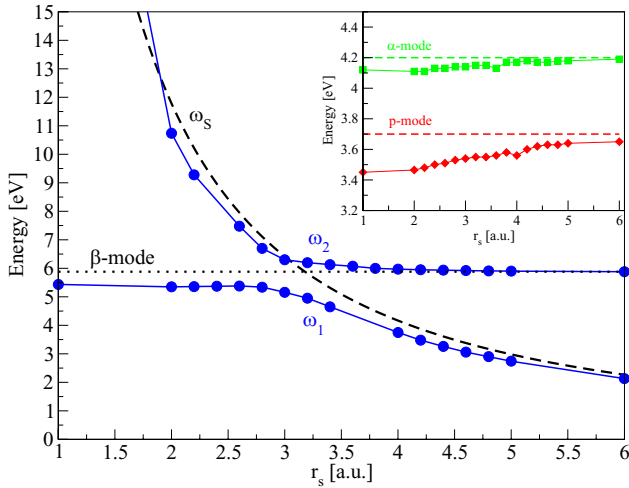


Figure 3. Avoided crossing behaviour of the β exciton in the anthracene molecule and surface plasmon in the adjacent metallic surface. Blue dots: energy of the most intensive peaks appearing in the anthracene absorption spectra (taken from spectra in figure 2) when the incident electromagnetic field is y polarized (i.e. energy of β exciton–surface plasmon coupled modes). Black dashed line: Drude surface plasmon branch (19). Black dotted line: The energy of the β exciton in a gas phase molecule. Inset: energy of anthracene p exciton (red diamonds) and anthracene α exciton (green squares) as a function of the adjacent surface Wigner Seitz radius r_s . The separation between the molecular plane and the *jellium* edge is chosen to be $z_0 = 6$ a.u.

located partially in the molecule and partially in the metallic surface. For even lower r_s (below 2.6) we can again see surface plasmon and β exciton peaks, with switched energy positions now, which is known as the avoided crossing behaviour, and is illustrated in the following figure 3.

In figure 2 we can also see that the width of the β exciton is strongly affected by the adjacent *jellium* surface. For example, if we look at the most prominent peaks for $3.4 < r_s < 4$, which can still be distinguished as β excitons, we can see that it is possible to fit them to the Lorentzian

$$A(\omega) \sim \frac{\Gamma}{(\omega - \omega_{\text{ex}})^2 + \Gamma^2}, \quad (18)$$

where Γ is the exciton decay width and ω_{ex} represents renormalized exciton energy. For $r_s = 3.4$ we obtained a decay width of $\Gamma = 273$ meV, suggesting that the β exciton decays very fast to the electronic modes in the metallic surface. A similar effect occurred for all bright modes in benzene, terylene and fullerene [11, 30, 37]. This proves that the dominant decaying channel is the excitation of the electron–hole pairs in the metallic surface. Figure 2 also shows that the exciton decay width increases as r_s decreases. Figure 2 inset shows exactly how the β exciton decay width depends on r_s . We can see that the exciton line-shape is infinitely narrow for $r_s > 5$. This is because the spectral weight of the electron–hole continuum is predominantly placed below the plasmon frequency ω_S [29]. Therefore, for $r_s < 3.5$, when $\omega_S > \omega_\beta$ the β exciton efficiently decays to a wide electron–hole continuum, and vice versa for $r_s > 3.5$, when $\omega_S < \omega_\beta$ its decay to the electron–hole becomes inefficient. It is interesting to note that the metallic surface does not affect the p and α exciton width.

The blue dots in figure 3 represent the peaks appearing in the y polarized light absorption spectra (some of them are marked by blue dots in figure 2), corresponding to β exciton–surface plasmon coupled modes, as a function on the Wigner Seitz radius r_s . The separation between the molecular plane and the *jellium* edge is chosen to be $z_0 = 6$ a.u. The energy of the gas phase β exciton is denoted by the black dotted line and the Drude surface plasmon branch

$$\omega_S = 33.327r_s^{3/2} \text{ [eV]} \quad (19)$$

is denoted by the black dashed line. Analysing the positions of the peaks, we can see that in the region $2.5 < r_s < 3.5$ the β exciton and the surface plasmon show the above mentioned avoided crossing behaviour. Examining the curves from right to left, i.e. from large r_s /low electron density towards small r_s /high electron density, we can see that the β exciton starts as a gas phase molecular exciton and finishes as a surface plasmon. On the other hand, the surface plasmon at first disperses as (19) and ends up slightly below the gas phase β exciton branch. This behaviour undoubtedly suggests strong β exciton–surface plasmon coupling in the region $2.5 < r_s < 3.5$. What is surprising here is that in the region $2.8 < r_s < 3.2$ the molecule supports two equally intense optically active modes (denoted by ω_1 and ω_2 in figure 2) where one of them can be attributed to surface plasmon. In other words, when the molecule is in the gas phase it absorbs light at ω_β , however in the vicinity of surfaces the molecule starts absorbing light at two frequencies ω_1 and ω_2 (also denoted in figure 3) which is a consequence of hybridization between ω_β and ω_S . The physical situations occurring here can be briefly described as follows. When the light hits the molecule it induces dipole active charge density oscillation, β exciton. Such charge oscillations produce a relatively strong and long range electric field around the molecule. Therefore if the surface is near, the molecule behaves as an oscillating dipole which can induce charge density oscillations in the metallic surface. Moreover, the metallic surface supports self-sustaining charge density oscillation, surface plasmon, which can be excited by a longitudinal probe such as a dipole. Therefore, the molecular dipole creates a sort of image in the surface, interacts with it and creates coupled modes $\omega_{1,2}$. For the mode ω_1 molecular and surface dipoles (inter-facial dipoles) oscillate out of phase and for mode ω_2 they oscillate in phase. It is especially intriguing that the surface actually stimulates the molecule to support one additional bright mode, which definitely opens many possibilities for the manipulation of the optical activity of the molecule.

The green squares in the inset of figure 3 show the energies of the anthracene α exciton as a function of the adjacent surface Wigner Seitz radius r_s . These energies are obtained by following low energy peaks of y polarized light absorption spectra (one of them is marked by the green arrow in figure 2). The energy of α exciton in vacuum is denoted by the green dashed line, and we can see that the presence of the surface barely changes the energy of the α exciton at all with respect to its vacuum value. Red diamonds in the figure 3 inset show the energies of anthracene p exciton (or anthracene optical gap) as a function of the adjacent surface Wigner Seitz radius r_s ,

and the red dashed line denotes the energy of the p exciton in vacuum. These energies are obtained by following the peaks of x polarized light absorption spectra (one of them is marked by the red arrow in figure 2). The energy of the p exciton also depends very weakly on the Wigner Seitz radius r_s . However, for metallic surfaces with a high electronic density, for $r_s = 1 - 2$, it underestimates the vacuum value for about 250 meV, or about 7%. By observing the spectral line-shape it is obvious that the p exciton does not hybridize with the surface exciton, i.e. the hybridization shift does not change the exciton energy. However, the exciton energy is defined by two other important factors: one is the energy of quasiparticle states in the HOMO–LUMO sector and the other is the strength of the electron–hole attraction. The metallic surface reduces the HOMO–LUMO gap but at the same time it weakens the electron–hole attraction, and the competition between these two effects defines the final exciton energy. In our previous analysis of benzene on a silver/gold surface ($r_s = 3$) [11] we showed that these two effects almost completely cancel out and the exciton energies remained unchanged. However, in this case, a more dense adjacent electron gas screens the molecular states more efficiently and therefore the reduction of the HOMO–LUMO gap is stronger than the weakening of the electron–hole attraction. The same trend can be noticed for the α exciton as well, but the reduction is smaller (about 90 meV).

Black dots in figure 4 represent the anthracene HOMO–LUMO gap obtained using the dynamical G_0W_0 corrected by (14) and (15), as a function of the molecule’s distance z_0 from the *jellium* surface with the electronic density corresponding with $r_s \approx 3.0$ a.u.. Blue squares show the HOMO–LUMO gap corrected using simple image theory which excludes dynamical effect in (14) and (15). This model assumes that the gas phase HOMO–LUMO gap is simply corrected by [18, 30]:

$$\frac{1}{2} \left\{ \Delta W_{LL}^{LL}(\omega = 0) + \Delta W_{HH}^{HH}(\omega = 0) \right\} \quad (20)$$

where $L = 33$ is the LUMO and $H = 34$ is the HOMO. We can see that this simple result agrees surprisingly well with the full dynamic G_0W_0 correction down to the distance from the metal surface of $z_0 \approx 6.0$ a.u.. This means that the surface field does not create virtual transitions ($j \neq i$ in (14) and (15)). Therefore, the HOMO and LUMO behave as rigid charge distributions $|\psi_H|^2$ and $|\psi_L|^2$ screened by the static induced potential $\Delta W(\omega = 0)$. Red diamonds show the HOMO–LUMO gap when the HOMO and LUMO energies are corrected by the image potentials $+\frac{e^2}{4(z_0 - z_{\text{im}})}$ and $-\frac{e^2}{4(z_0 - z_{\text{im}})}$, respectively. The effective image plane (measured from the *jellium* edge $z = 0$) can be obtained by using a surface excitation propagator as

$$z_{\text{im}} = \frac{1}{2} \left. \frac{dD(Q, \omega = 0)}{dQ} \right|_{Q=0}. \quad (21)$$

For $r_s = 3$ the effective image plane is $z_{\text{im}} = 0.91$ a.u. We find that this very simple approach first underestimates and then for $z_0 \geq 12$ a.u. overestimates the HOMO–LUMO gap. This is reasonable because anthracene is an elongated planar

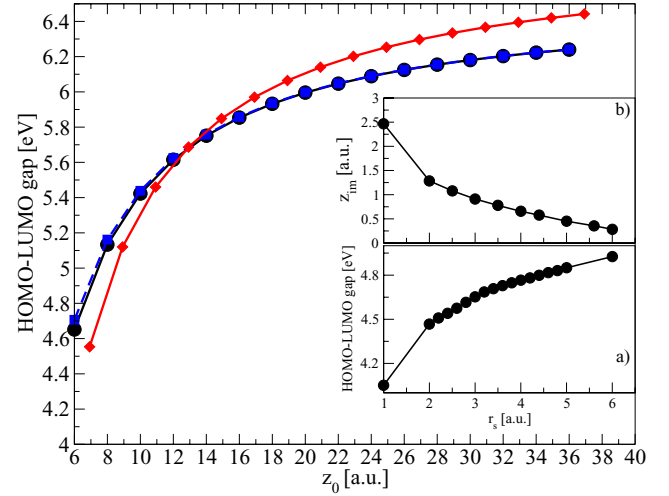


Figure 4. HOMO–LUMO gap of the anthracene molecule as a function of the distance z_0 from a metallic surface. Black dots: full dynamical G_0W_0 calculation corrected by equations (14) and (15). Blue squares: image theory of equation (20). Red diamonds: HOMO and LUMO energies corrected by the image potential $(\pm \frac{e^2}{4(z_0 - z_{\text{im}})})$. The metallic surface Wigner Seitz radius is $r_s = 3$ and the corresponding image plane position is $z_{\text{im}} = 0.91$ a.u. Inset (a) HOMO–LUMO gap of anthracene as a function of r_s . The separation between the molecular plane and the *jellium* edge is $z_0 = 6$ a.u.. Inset (b) position of the effective image plane z_{im} (measured relatively to the *jellium* edge $z = 0$) as a function of r_s obtained from equation (21).

molecule, and for the considered separations $|\psi_H|^2$ and $|\psi_L|^2$ still does not behave as a positive or negative point charge, i.e. higher multipoles still contribute.

The black dots in the inset of figure 4(a) show the quasiparticle HOMO–LUMO gap obtained using the dynamical G_0W_0 corrected by (14) and (15), as a function of the Wigner–Seitz radius r_s of the adjacent surface. We can see that the vicinity of the metallic surface significantly reduces the molecule HOMO–LUMO gap with respect to its gas phase value. The HOMO–LUMO gap reduction is -2.8 eV for $r_s = 1$ and -1.9 eV for $r_s = 6$. In the region $r_s = 1 - 3$ the HOMO–LUMO gap first rapidly increases and after that it slowly saturates to the vacuum value. This behaviour also agrees well with the proposed image theory description of the HOMO–LUMO shift. Namely, the effective image plane z_{im} depends on the Wigner Seitz r_s in the way that it decreases as r_s increases, as shown in figure 4(b) inset. Therefore for lower r_s the effective image plane is further from the *jellium* edge, i.e. closer to the molecule and the HOMO–LUMO gap reduction is larger, and vice versa, as r_s increases, the image plane moves away from the molecule and the HOMO–LUMO gap increases. The evidence that the described mechanism of a moving image plane is indeed responsible for the HOMO–LUMO gap change is a nice mirror symmetry of the graphs presented in figures 4(a) and (b) insets. Figure 5 shows the anthracene optical absorption spectra as a function of the incident light frequency ω and for various distances $z_0 = 6, 8, 10, \dots, 36$ a.u. from the adjacent *jellium* surface. The graph on the bottom corresponds to $z_0 = 6$ a.u. and for each subsequent graph z_0 increases by 2 a.u., so the

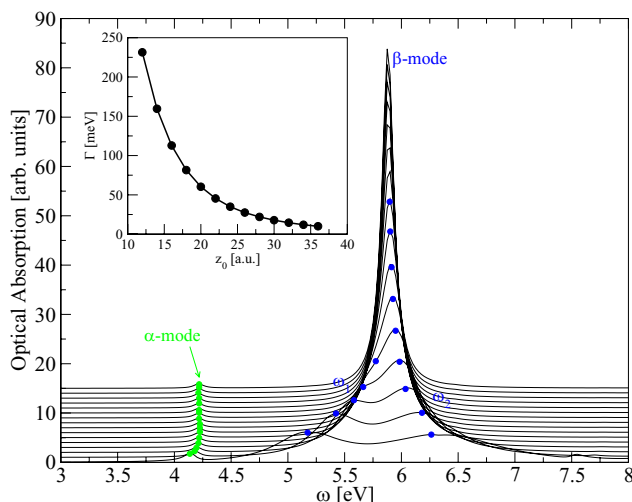


Figure 5. Anthracene optical absorption spectra as functions of the incident light frequency ω and for various distance $z_0 = 6, 8, 10, \dots, 36$ a.u. (from bottom to top). Incident light is y polarized, i.e. $\mathbf{e} = \mathbf{e}_y$ and $r_s = 3$. Inset: β exciton decay width Γ as a function of molecule metallic surface separation z_0 .

graph on the top shows the spectrum for $z_0 = 36$ a.u. The Wigner Seitz radius of the metallic surface is chosen to be $r_s = 3$. The incident light is polarized along a long molecular axis, i.e. $\mathbf{e} = \mathbf{e}_y$ which means that the high intensity peaks in the spectra represent the β exciton-surface plasmon coupled modes. The figure clearly shows how the anthracene β exciton splits to coupled modes ω_1 and ω_2 (marked by blue dots) as the molecule approaches the metallic surface. This undoubtedly proves the strong hybridization between the β exciton and the surface plasmon. Another consequence of the metallic surface is the strong decay of the β exciton to the electron-hole excitations. In the weak coupling region, $z_0 \geq 12$ a.u., when the surface plasmon still does not affect the β exciton energy, it already significantly decays to the electron-hole excitations. For example, the β exciton decay width, obtained by a fit to the Lorentzian (18), for $z_0 = 12$ a.u. is $\Gamma = 231$ meV.

Figure 5 inset shows β exciton decay width as a function of the distance z_0 . We can see that the exciton width decreases exponentially as z_0 increases. This is expected behaviour, since for a particular wave vector Q the induced potential (11) decreases as e^{-2Qz_0} , so for large z_0 only the long-wavelength ($Q \rightarrow 0$) excitations, such as collective modes, can reach the molecule. However, it is interesting to note that even at this long range separation ($z_0 \approx 20$ a.u.), the β exciton still decays ($\Gamma \approx 50$ meV) significantly.

4. Conclusion

In this paper we demonstrated how the vicinity of the various metallic surfaces influence the HOMO-LUMO gap, and the bright excitons in the anthracene ($C_{14}H_{10}$). We showed that the p and α excitons weakly interact with surface excitations, while the most intensive β exciton considerably hybridizes with surface plasmon. We showed that for a particular *jellium* surface ($r_s = 3$), corresponding to silver or gold surfaces,

the β exciton splits into two bright modes. For the non-contact separations ($z_0 \approx 12$ a.u.) and $r_s = 3$ the β exciton decays extraordinarily fast ($\Gamma \approx 200$ meV) to the electron-hole excitations in the metallic surface. For $r_s > 5$ the β exciton interacts very weakly with the surface, and its energy and width Γ reduces to its vacuum value. We demonstrated that the simple image theory arguments are sufficient to explain the HOMO-LUMO gap shift. For example, the HOMO and LUMO states near a metallic surface behave as statically screened rigid orbitals. Moreover, we demonstrated that the position of the effective image plane z_{im} of the *jellium* surface dominantly influences the HOMO-LUMO gap shift. This theoretical research provides insight into methods for manipulation of the electronic and optical spectra of an organic molecule or a molecular crystal by combining them with various metallic or semi-metallic nanoparticles. This issue is becoming of crucial importance today in photovoltaic applications.

Acknowledgments

V D is grateful to the Donostia International Physics Center (DIPC) and to P M Echenique for their hospitality during various stages of this research. The authors also thank I Kupčić and D J Mowbray for useful discussions.

References

- [1] Pandey A K and Nunzi J-M 2006 *Appl. Phys. Lett.* **89** 213506
- [2] Girtan M, Dabos-Seignon S and Stanculescu A 2009 *Vacuum* **83** 1159
- [3] Cui T and Liang G 2005 *Appl. Phys. Lett.* **86** 064102
- [4] Kim D H, Lee D Y, Lee H S, Lee W H, Kim Y H, Han J I and Cho K 2007 *Adv. Mater.* **19** 678
- [5] Anker J N, Hall W P, Lyandres O, Shah N C, Zhao J and Van Duyne R P 2008 *Nat. Mater.* **7** 442
- [6] Marrocchi A, Silvestri F, Seri M, Facchetti A and Taticchia A 2009 *Chem. Commun.* **11** 1380
- [7] Liu C, Cai W, Guan X, Duan C, Xue Q, Ying L, Huang F and Cao Y 2013 *Polym. Chem.* **4** 3949
- [8] Aazou S, A Ibral, White M S, Kaltenbrunner M, Glowacki E D, Egbe D A M, Sariciftci N S and Assaid E L M 2013 *J. Optoelectron. Adv. Mater.* **13** 395
- [9] Ferguson A J, Blackburn J L and Kopidakis N 2013 *Mater. Lett.* **90** 115
- [10] Zhuang T, Wang X-F, Sano T, Hong Z, Yang Y and Kido J 2013 *Appl. Phys. Lett.* **103** 203301
- [11] Despoja V, Lončarić I, Mowbray D J and Marušić L 2013 *Phys. Rev. B* **88** 235437
- [12] Hedin L 1965 *Phys. Rev.* **139** A796
- [13] Strinati G 1984 *Phys. Rev. B* **29** 5718
- [14] Hybertsen M S and Louie S G 1986 *Phys. Rev. B* **34** 5390
- [15] Rohlfling M and Louie S G 1998 *Phys. Rev. Lett.* **81** 2312
- [16] Rohlfling M and Louie S G 2000 *Phys. Rev. B* **62** 4927
- [17] Onida G, Reining L and Rubio A 2002 *Rev. Mod. Phys.* **74** 601
- [18] Neaton J B, Hybertsen M S and Louie S G 2006 *Phys. Rev. Lett.* **97** 216405
- [19] Spataru C D 2013 *Phys. Rev. B* **88** 125412
- [20] Mallocci G, Cappellini G, Mulas G and Mattoni A 2011 *Chem. Phys.* **384** 19
- [21] Mallocci G, Mulas G, Cappellini G and Joblin C 2007 *Chem. Phys.* **340** 43

- [22] Kadantseva E S, Stott M J and Rubio A 2006 *J. Chem. Phys.* **124** 134901
- [23] Yannoulis P, Frank K H and Koch E E 1991 *Surf. Sci.* **241** 325
- [24] Sun D *et al* 2010 *Phys. Rev. B* **82** 201410
- [25] Stokbro K and Smidstrup S 2013 arXiv:1308.0969
- [26] Liu W, Carrasco J, Santra B, Michaelides A, Scheffler M and Tkatchenko A 2012 *Phys. Rev. B* **86** 245405
- [27] Mete E, Demiroglu I, Fatih Danisman M and Ellialtioglu S 2010 *J. Phys. Chem. C* **114** 2724
- [28] Lončarć I and Despoja V 2014 *Phys. Rev. B* **90** 075414
- [29] Marušić L, Despoja V and Sunjić M 2006 *J. Phys.: Condens. Matter* **18** 4253
- [30] Despoja V and Mowbray D J 2014 *Phys. Rev. B* **89** 195433
- [31] Kupčić I, Rukelj Z and Barišić S 2013 *J. Phys.: Condens. Matter* **25** 145602
- [32] Marušić L and Šunjić M 2001 *Phys. Scr.* **63** 336
- [33] Ashcroft N W and Mermin N D 1976 *Solid State Physics* (Orlando, FL: Harcourt College Publishers)
- [34] Giannozzi P *et al* 2009 *J. Phys.: Condens. Matter* **21** 395502
- [35] Perdew J P, Chevary J A, Vosko S H, Jackson K A, Pederson M R, Singh D J and Fiolhais C 1992 *Phys. Rev. B* **46** 6671
- [36] Rozzi C A, Varsano D, Marini A, Gross E K U and Rubio A 2006 *Phys. Rev. B* **73** 205119
- [37] Despoja V and Mowbray D J 2014 submitted